J Mater Sci (2006) 41:5890–5899
DOI 10.1007/s10853-006-0265-7

Optimization of hardening of Al–Zr–Sc cast alloys

N. A. Belov · A. N. Alabin · D. G. Eskin · V. V. Istomin-Kastrovskii

Received: 29 March 2005 / Accepted: 13 October 2005 / Published online: 6 July 2006

Abstract The effects of composition, cooling rate after the end of solidification, and annealing regime on the structure and hardening of binary and ternary alloys of the Al–Sc–Zr system are studied. The liquidus in Al–Sc–Zr alloys is experimentally assessed in order to facilitate the correct choice of casting temperatures. The precipitation during slow cooling after the end of solidification causes hardening in the as-cast state and decreases the hardening effect during annealing. It is shown that the full hardening ability of precipitates can be achieved only upon their homogeneous distribution in the matrix. The optimum total concentration of Sc and Zr in aluminium alloys should be about 0.3 wt% at the ratio Zr:Sc ≥ 2. That allows conventional casting temperatures and considerable hardening during annealing.

Introduction

Scandium is one of the most promising additions to aluminium alloys, enabling structure refinement and hardening due to the formation of precipitates of the equilibrium Al_3Sc ($L1_2$) phase during solidification and upon decomposition of supersaturated solid solution. The maximum effect of precipitation hardening can be achieved during annealing in the temperature range from 300 °C to 350 °C [1]. At higher temperatures, the precipitates coarsen and lose coherency, which decreases the hardening effect.

Commercial wrought aluminium alloys based on the Al–Mg and Al–Li–Mg systems and containing scandium additions have been developed in the USSR in the 1970–1980s. These alloys utilize the following mechanisms: grain refinement in as-cast billets, structural hardening due to hindered recrystallization, and precipitation hardening (some of Al–Mg alloys) [1]. It was shown that joint introduction of scandium with zirconium resulted in the retarded decomposition of supersaturated solid solutions and the slowed down coarsening of hardening particles (hence, allowed one to increase the allowable temperature of solution treatment for commercial alloys and to decrease the necessary concentration of scandium in an alloy). In such alloys, zirconium partially substitutes for scandium in the Al_3Sc phase, forming the $Al_3(ScZr)$ phase [1] or composite particles with Al_3Sc core and Zr-enriched shell [2, 3]. In this case, the optimum concentrations are 0.2–0.3% Sc and 0.15% Zr [1]. In addition, zirconium forms its own phase—Al_3Zr—that may exist in the stable, tetragonal ($D0_{23}$) modification or in the metastable, cubic ($L1_2$) modification. A bimodal distribution of particles after high-temperature decomposition of a supersaturated solid solution is reported by Toropova et al. [1] and attributed to the formation of two $L1_2$ phases, Al_3Sc and Al_3Zr. Whereas other researchers observed the precipitation of a single $L1_2$ phase, designated as $Al_3(ScZr)$ in ternary Al–Sc–Zr alloys, e.g., [2–4]. In this case, the higher temperature stability of metastable $Al_3(ScZr)$ particles is related to homogeneous nucleation, lesser lattice misfit with the matrix [4], slower diffusion of Zr in (Al) [1], and changed composition of the particle/matrix interface [2, 3]. Addition of Sc to Al–Zr

N. A. Belov · A. N. Alabin · V. V. Istomin-Kastrovskii
Moscow Institute of Steel and Alloys, Leninsky prosp. 4, Moscow 119049, Russia

D. G. Eskin (✉)
Netherlands Institute for Metals Research, Mekelweg 2, 2628CD Delft, The Netherlands
e-mail: d.g.eskin@tudelft.nl

alloys changes the mode of nucleation of dispersoids from heterogeneous to homogeneous, increases the density of precipitation, and decreases the average size of particles [5]. Moreover, due to the opposite partitioning of Sc (enriches the dendrite edges) and Zr (enriches the central portion of dendrite branches) during solidification, the ternary alloys exhibit much more homogeneous distribution of precipitates after decomposition of the supersaturated solid solution as has been experimentally demonstrated elsewhere [6]. If the supersaturated solid solution contains 0.5–0.8% Zr, then the metastable $L1_2$ Al_3Zr phase can be an efficient hardener [7, 8]. Zirconium is much cheaper than scandium, and the strengthening effect from the Al_3Zr phase can be retained to higher temperatures, i.e., up to 450 °C, which allows one to use this addition in alloys with a low solidus, e.g., in Al–Zn–Mg alloys. On the other hand, the introduction of such a considerable amount of Zr in (Al) requires rather high casting temperatures (above 800–850 °C) which is not suitable for alloys containing such volatile components as magnesium, zinc, or lithium.

The attractive alloy composition should combine the following features:

- hardening effect is comparable to that in aluminium alloys containing 0.2–0.3% Sc;
- hardening effect is stable at temperatures as high as 450 °C;
- concentration of scandium is decreased to 0.1%; and
- casting temperature should be less than 800 °C, better below 770 °C.

The aim of this work was to optimize the alloy composition and annealing regimes with respect to the structure and hardening of Al–Sc–Zr alloys.

Experimental

Nine experimental alloys were prepared in an electric furnace using 99.99% pure aluminium and Al–2% Sc and Al–3.5% Zr master alloys. The compositions of the alloys compose a matrix as shown in Fig. 1. The alloys were cast from 850 °C into a steel mould with internal dimensions of 15 × 30 × 180 mm. The melt temperature was chosen to be above the highest possible liquidus temperature in order to prevent the formation of primary crystals. The liquidus isotherms are shown in Fig. 1a. These isotherms were experimentally constructed using the nine experimental alloys and two additional binary Al–Zr alloys containing 0.8% and 1% Zr. Samples 15 g in weight were heated in alumina crucibles in the temperature range from 670 °C to 900 °C. After 1-h exposure at a given temperature, the crucibles with melt were quenched in cold water. The

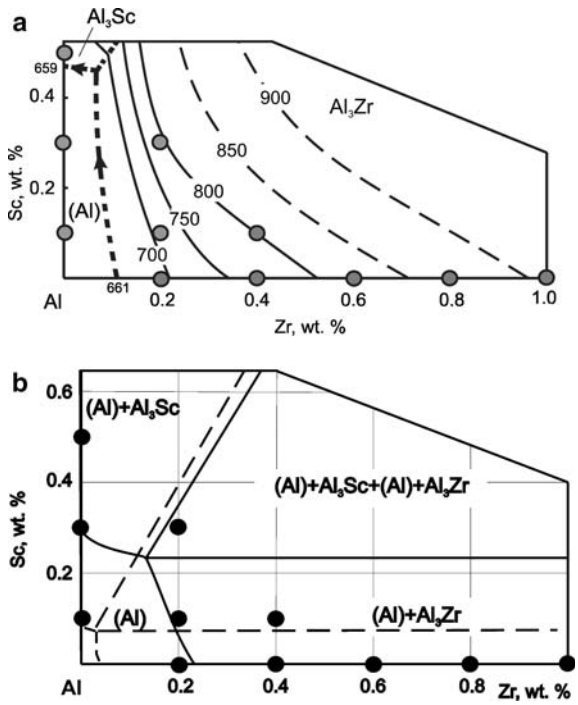

Fig. 1 (**a**) Liquidus isotherms and (**b**) isothermal sections at 640° (solid lines) and 450 °C (dashed lines) of the Al–Sc–Zr phase diagram. Back dots show experimental alloys

structure was examined in the vertical cross-section of the sample along the entire height, as primary crystals might settle during holding in the slurry state. The presence or absence of these primary crystals testified for the region—slurry or liquid—where the alloy was at the given temperature [9].

Upon casting into a preheated mould the initial cooling rate in the solid state was 7 K/s (V_{c1}) and when casting into a cold mould the initial cooling rate in the solid state was 20 K/s (V_{c2}). The change of cooling rates with the decreasing temperature in the solid state is illustrated in Table 1. The cooling rates in the solidification range were somewhat higher and sufficient to prevent the formation of primary or eutectic crystals during solidification and to assure the formation of a single-phase (supersaturated) solid solution of Sc or/and Zr in (Al) [7, 8].

Table 1 Variation of cooling rates with the decreasing temperature in the solid state upon cooling in preheated (V_{c1}) and cold (V_{c2}) moulds

T, °C	Instantaneous cooling rate, K/s	
	V_{c1}	V_{c2}
650 (just below solidus)	7	20
550	4.9	16
450	0.3	5.3
350	0.07	2.2

The structure was examined in optical (OM Neophot 30), scanning electron (SEM JSM-35CF) and transmission electron (TEM JEM 2000EX) microscopes. For microstructure examination, the samples were polished in a perchloric acid–ethanol electrolyte and additionally oxidized in a 5% water solution of HBF_4 at 20 VDC for revealing the grain structure. Foils for transmission electron microscopy were electrolytically thinned in a perchloric acid–ethanol solution and examined in the TEM at a voltage of 120 kV. Phase identification was performed using selected-area diffraction patterns.

All alloys after the end of solidification were single-phase as has been confirmed by the structure examination in optical and scanning electron microscopes.

The cast samples were annealed in an electric furnace in the temperature range from 250 °C to 640 °C using stepped modes as given in Table 2. Such a technique of annealing allowed us to accelerate the experiments. Alloys containing only scandium or both scandium and zirconium were annealed starting from 250 °C, whereas for the binary Al–Zr alloys the first step of annealing was at 300 °C as these alloys do not harden at lower temperatures [7, 8]. The Brinell hardness was measured using standard equipment at a load of 2,500 N, ball indenter of 5-mm diameter, and 30-s duration of the indentation.

Results and discussion

The formation of supersaturated solid solution during solidification of aluminium alloys containing transition metals is a function of two parameters: the initial temperature of the melt and the cooling rate upon solidification and in the solid state. With increasing the cooling rate during solidification the concentration boundary at which primary crystals start to form shifts towards larger concentrations of transition metal [1]. This can be illustrated by a schematic non-equilibrium Al–Zr phase diagram as shown in Fig. 2. Similar diagrams but for the formation of the metastable Al_3Zr phase and a supersaturated (Al) solid solution have been reported earlier by Dobatkin [10] and

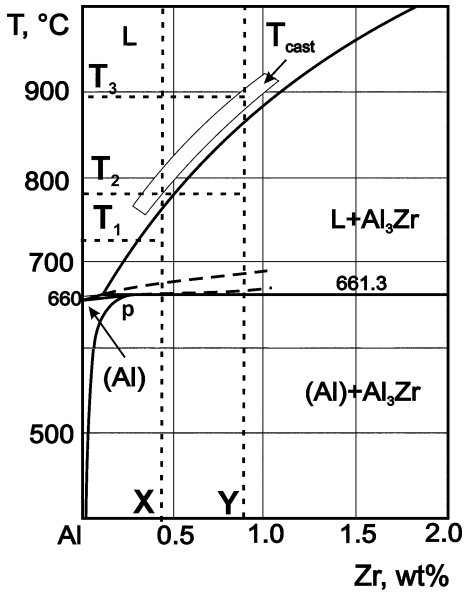

Fig. 2 Scheme showing equilibrium and non-equilibrium liquidus of Al–Zr alloys and illustrating the correct choice of casting temperatures and cooling rates during solidification for the complete introduction of Zr into supersaturated solid solution during solidification: T_2 and V_{c1} are correct for alloy X; and T_3 and V_{c2} are correct for alloy Y

Nes and Billdal [11]. With increasing the cooling rate V_c the liquidus and solidus lines for the solidification of aluminium solid solution are extended towards higher zirconium concentrations and the peritectic reaction does not occur under non-equilibrium solidification conditions. As a result, an anomalously supersaturated solid solution of Zr in (Al) can be formed. However, this phenomenon does not necessarily leads to the complete introduction of Zr into (Al) upon solidification. The additional condition for that is the absence of primary Al_3Zr crystals in the melt prior to the beginning of cooling. Obviously, the melt temperature and, therefore the casting temperature should be above the liquidus of the alloy. Otherwise, zirconium will be partially bound in primary crystals and cannot enter the supersaturated solid solution at any cooling rate during solidification. For example, temperature T_1 is too low for alloy X though cooling rate can be sufficient for the formation of a

Table 2 Annealing regimes

Regime	Steps of annealing*
S250	250 °C, 3 h
S300	250 °C, 3 h + 300 °C, 3 h
S350	250 °C, 3 h + 300 °C, 3 h + 350 °C, 3 h
S400	250 °C, 3 h + 300 °C, 3 h + 350 °C, 3 h + 400 °C, 3 h
S450	250 °C, 3 h + 300 °C, 3 h + 350 °C, 3 h + 400 °C, 3 h + 450 °C, 3 h
S500	250 °C, 3 h + 300 °C, 3 h + 350 °C, 3 h + 400 °C, 3 h + 450 °C, 3 h + 500 °C, 3 h
S550	250 °C, 3 h + 300 °C, 3 h + 350 °C, 3 h + 400 °C, 3 h + 450 °C, 3 h + 500 °C, 3 h + 550 °C, 3 h
S600	250 °C, 3 h + 300 °C, 3 h + 350 °C, 3 h + 400 °C, 3 h + 450 °C, 3 h + 500 °C, 3 h + 550 °C, 3 h + 600 °C, 3 h
S640	250 °C, 3 h + 300 °C, 3 h + 350 °C, 3 h + 400 °C, 3 h + 450 °C, 3 h + 500 °C, 3 h + 550 °C, 3 h + 600 °C, 3 h + 640 °C, 3 h

*The first step for binary Al–Zr alloys is 300 °C (step at 250 °C is not used)

supersaturated solid solution. Proper casting temperature T_2 for alloy X is absolutely unsuitable for alloy Y at any cooling rate. For alloy Y, temperature T_3 should be chosen for the formation of a supersaturated solid solution containing all zirconium, providing that the cooling rate is sufficiently high. All these speculations demonstrate how important is to know the liquidus temperature of alloys. Unfortunately, the liquidus surface in the Al–Sc–Zr system is not readily available from the literature. Therefore, we made our estimation based on the experimental results obtained as described in Experimental. We also took into account the temperatures of invariant reactions from binary phase diagrams and experimental polythermal sections reported elsewhere [1]. The experimental liquidus isotherms are given in Fig. 1a. The liquidus temperatures for some experimental alloys are given below:

Alloy	Al–0.1% Sc–0.2% Zr	Al–0.1% Sc–0.4% Zr	Al–0.3% Sc–0.2% Zr
Liquidus, °C	690–700	785–795	785–795

The as-cast structures of all experimental alloys cooled at two cooling rates do not exhibit any primary crystals, which shows that all these alloys ended solidification as a single-phase solid solution. However, the absence of primary crystals does not necessarily mean that the supersaturated solid solution is retained upon further cooling in the solid state to room temperature. The evidence for that is given below.

Figure 3 shows the hardness of experimental alloys against the temperature of the last step of annealing.

There are three parameters to which we would like to pay attention to.

Firstly, the temperature range of effective hardening. In the case of binary Al–Zr alloys, this temperature range is between 350 °C and 450 °C (Fig. 3a). Binary Al–Sc alloys show a narrower temperature range of effective hardening, between 300 °C and 350 °C, almost no hardening can be observed above 450 °C (Fig. 3b). And ternary Al–Sc–Zr alloys gain the hardness in the temperature range between 350 °C and 450 °C (Fig. 3c). The main difference between binary Al–Zr and ternary Al–Sc–Zr alloys is more rapid hardening of the latter in the range of 300–350 °C. Recent publications reported the formation of complex $Al_3(ScZr)$ precipitates with the core enriched in scandium [2, 3]. This can explain the accelerated hardening in ternary alloys as compared to binary alloys. Scandium diffuses faster than zirconium in aluminium and forms clusters which then act as nucleation sites for the $Al_3(ScZr)$ phase.

Second parameter is the alloy composition. Hardening of binary Al–Zr alloys containing 0.2% Zr (that is maximum concentration in commercial aluminium alloys) is

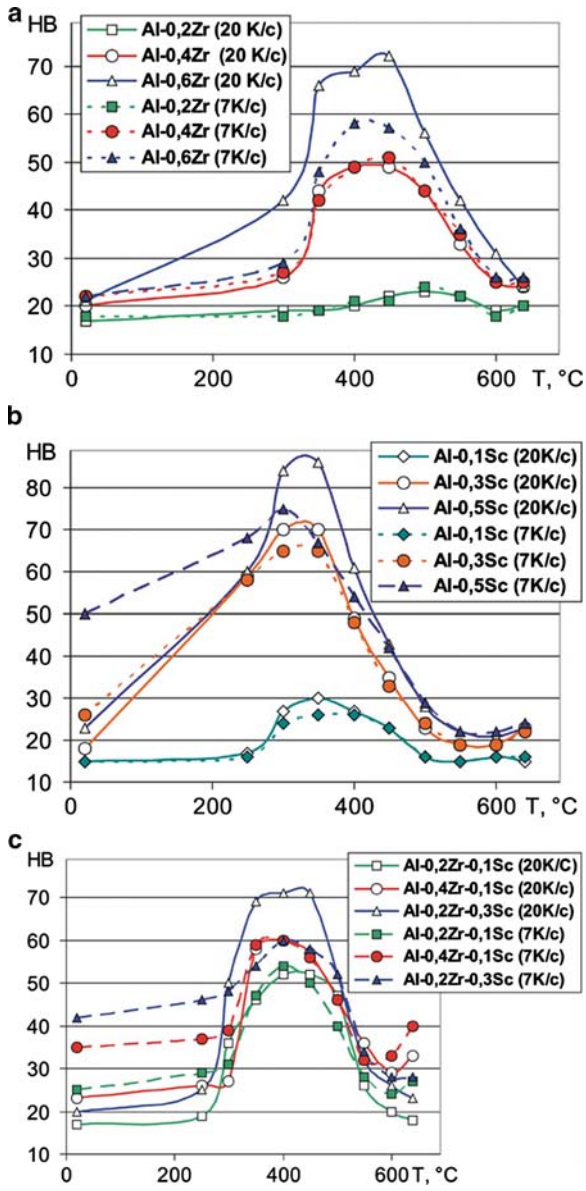

Fig. 3 Dependence of hardness on the composition, cooling rate in the solid state, and the temperature of the last annealing step (Table 1): (**a**) binary Al–Zr alloys; (**b**) binary Al–Sc alloys; and (**c**) ternary Al–Sc–Zr alloys

negligible, whereas 0.4% Zr produce a noticeable effect. Although a binary Al–0.1% Sc alloy shows some hardening, it can be considered rather weak. However, joint introduction of 0.2% Zr and 0.1% Sc gives much stronger effect than just arithmetic summation of individual contributions. The general tendency in all three groups of alloys is: the more the concentration of Sc and Zr, the larger the hardening.

And the third important variable in these dependences is the cooling rate after the end of solidification (difference in solid and dashed lines in Fig. 3). In binary Al–Zr alloys, slower cooling in the solid state does not affect the hard-

ness of as-cast material and the hardening in the alloys containing 0.2–0.4% Zr. However, the hardening is less in the Al–0.6% Zr alloy cooled at V_{c1} (7 K/s) as compared to the same alloy but cooled at V_{c2} (20 K/s). The effect of the cooling rate is much more pronounced in Al–Sc alloys, being larger in more alloyed materials. The effect is twofold. Firstly, the as-cast alloy is harder after being slowly cooled in the solid state, the difference can be as large as two times (or appr. 30HB) for the Al–0.5% Sc alloy. And secondly, the maximum hardness reached after annealing of a slowly cooled alloy is less than that for a faster cooled alloy (a difference of appr. 10–15HB for the Al–0.5% Sc alloy). Similar effects are observed in ternary Al–Sc–Zr alloys, the hardness in the as-cast state being now the function of both the cooling rate and the concentration of the alloying elements.

The effect of alloy composition and cooling rate in the solid state on the hardening of experimental alloys is demonstrated in Fig. 4 for three different states, i.e., as-cast (Fig. 4a, b), annealed to the maximum hardness (Fig. 4c, d), and annealed with the last annealing stage at 500 °C (S500 in Table 2) (Fig. 4e, f). The last regime is practically important as 500 °C is close to typical temperatures of solution treatment of most commercial aluminium alloys. The analysis of these dependences yields the following conclusions. The effect of alloying elements on the hardness in the as-cast state is very small at the higher cooling rate but becomes considerable at the lower cooling rate, the influence of scandium being much more pronounced than that of zirconium (Fig. 4a, b). After annealing to the maximum hardness (the annealing regimes are different for different alloys, see Fig. 3), the effect of both alloying elements on the hardness is strong and comparable for both cooling rates (Fig. 3c, d). On increasing the annealing temperature (last stage at 500 °C), the effect of alloying elements on the hardness is similar at both cooling rates, but now the compositional range of harder alloys is located closer to the Al–Zr side of the concentration triangle.

The presented dependences give us some ground to speculate that the slower cooling rate may result in precipitation of hardening particles during cooling after the end of solidification, which causes the increased hardness in the as-cast state, and somewhat decreases the hardening effect after annealing to the maximum hardness. An examination of the internal structure of the examine alloys is, however, required to justify such a discussion.

Binary Al–Zr alloys annealed to the maximum hardness (regime S450 in Table 2) demonstrate rather inhomogeneous distribution and large spacing of Al_3Zr particles in the Al–0.2% Zr alloy as shown in Fig. 5a, whereas the precipitation becomes much more homogeneous and numerous in the Al–(0.4–0.6)% Zr alloys, see Fig. 5b–c. Note that the Al_3Zr phase is metastable (cubic $L1_2$) as has been confirmed by selected-area diffraction patterns, and its particles have a ''coffee-bean'' contrast (Fig. 5b) attesting for their coherency with the matrix. These difference in the distribution and precipitation density of hardening particles explains the observed hardening behaviour (see Fig. 3a).

Addition of 0.1% Sc to the Al–0.2% Zr alloy makes its structure after annealing to the maximum hardness (S400 in Table 2) similar to that observed for the Al–0.4% Zr alloy (Fig. 5b) only now the precipitating phase is likely to be $Al_3(ScZr)$ as shown in Fig. 6. Accordingly, a well-pronounced hardening effect is observed (see Fig. 3c). The structure of annealed binary Al–Sc alloys is well studied elsewhere and has not been the subject of this work [1, 12–15]. Literature data show that the formation of the Al_3Sc phase during cooling after the end of solidification may result in the homogeneous or discontinuous precipitation [12]. And Al_3Sc precipitates can retain the coherency at temperatures as high as 400 °C [1] and during hundreds of hours at 350 °C [13].

The Al–0.3% Sc–0.2% Zr alloy shows the most pronounced difference in the hardening behaviour with respect to the cooling rate after the end of solidification as well as the highest peak hardness, see Fig. 3c. The internal structure of this alloy was studied in detail. The structure of the alloy cooled after the end of solidification at V_{c1} exhibit all features of decomposition with rather inhomogeneous precipitation as can be seen in Fig. 7a. As a result of this precipitation, the as-cast alloy is hardened. After cooling at V_{c2}, the precipitation is much less pronounced, Fig. 7b. Accordingly the hardness of the alloy is lower but the alloy is more supersaturated in Sc and Zr. After annealing to the maximum hardness by regime S400, samples obtained at both cooling rates demonstrate intensive but rather inhomogeneous distribution of dispersoids as compared to the Al–0.1% Sc–0.2% Zr alloy (compare Fig. 6a and Fig. 7c, d). However, even this inhomogeneous precipitation results in considerable hardening. Logically, the hardening effect is higher in the alloy that has been more supersaturated before the beginning of precipitation, i.e., in the alloy cooled at V_{c2}.

In addition to the initial supersaturation of the solid solution, the distribution of precipitates and their volume fraction are important for hardening. The maximum hardness obtained on samples cooled at V_{c2} (20 K/s) can be correlated to the volume fraction of precipitates. As we showed the precipitation during cooling at this cooling rate was minimal. With taking into account that the equilibrium solubilities of Sc and Zr in (Al) at the given annealing temperatures are small, one can consider that both scandium and zirconium are completely bound in $L1_2$ dispersoids after annealing. The calculated maximum volume fractions of dispersoids in the experimental alloys are given

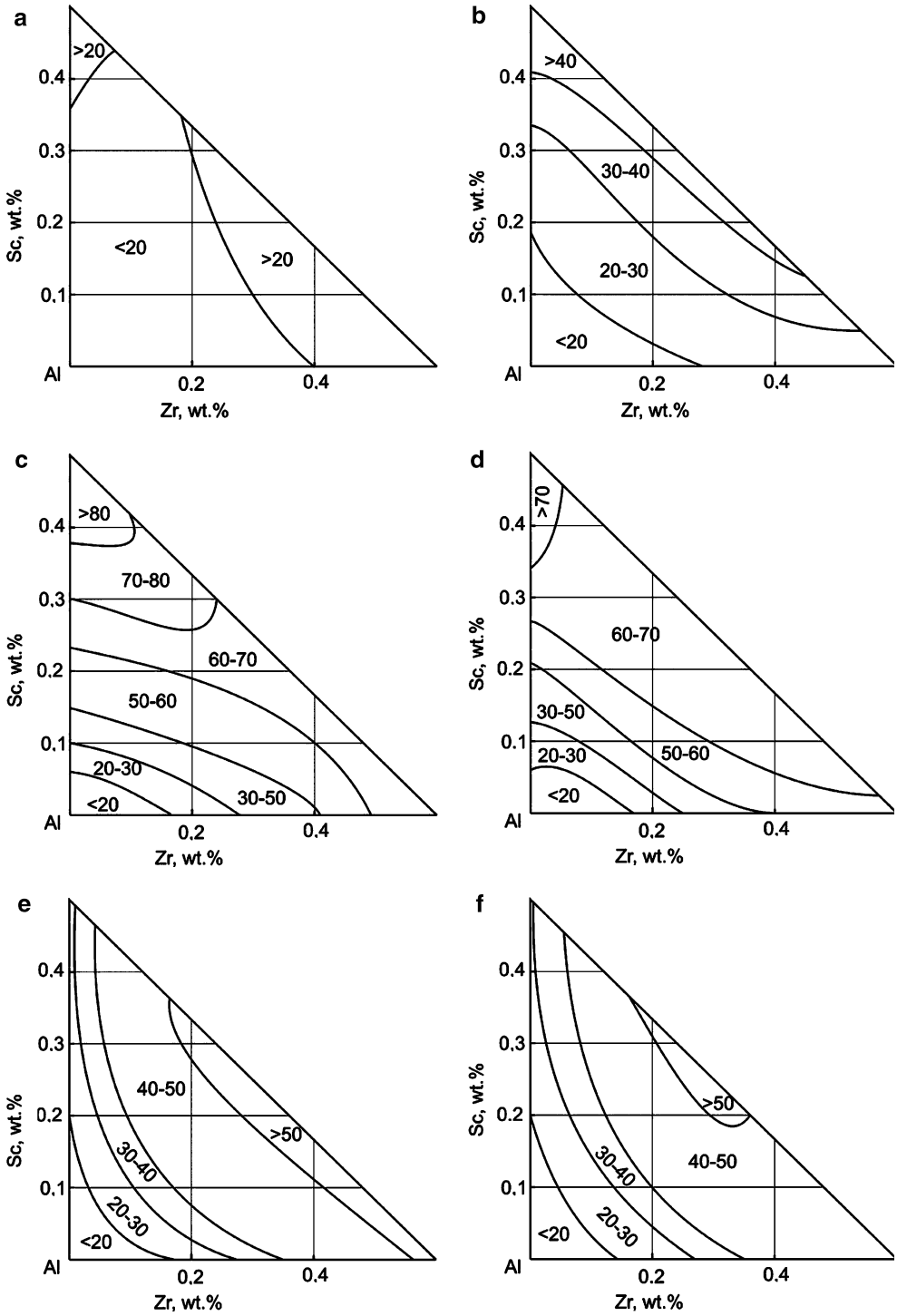

Fig. 4 Effect of composition, cooling rate in the solid state (Table 1), and the annealing regime on the hardness of experimental alloys: (**a**, **c**, **e**) cooling rate V_{c2}; (**b**, **d**, **f**) cooling rate V_{c1}; (**a**, **b**) as-cast condition; (**c**, **d**) maximum hardness; and (**e**, **f**) S500 (see Table 2). The isolines are the result of polynomial interpolation of experimental points that constitute a matrix as shown in Fig. 1

in Table 3. One can see that the concentration of Zr in the binary alloy should be twice the concentration of Sc to achieve the same volume fraction of precipitates. In other words, an alloy with 0.3% Sc should exhibit similar precipitation hardening level as an alloy with 0.6% Zr. This is confirmed by hardness measurements in Fig. 3c.

The experimental data on maximum hardness are put in Fig. 8 against the calculated volume fractions of precipitates. Two hardening mechanisms are possible in the alloys in question, subject to the coherency of particles, their size and interparticle spacing [4, 16]. The anti-phase boundary mechanism involves cutting of the particles by dislocations and assumes that the hardening is directly proportional to the volume fraction of precipitates. In the case of Orowan's mechanism of hardening when dislocations bow around the particles, the hardness should be inversely proportional to

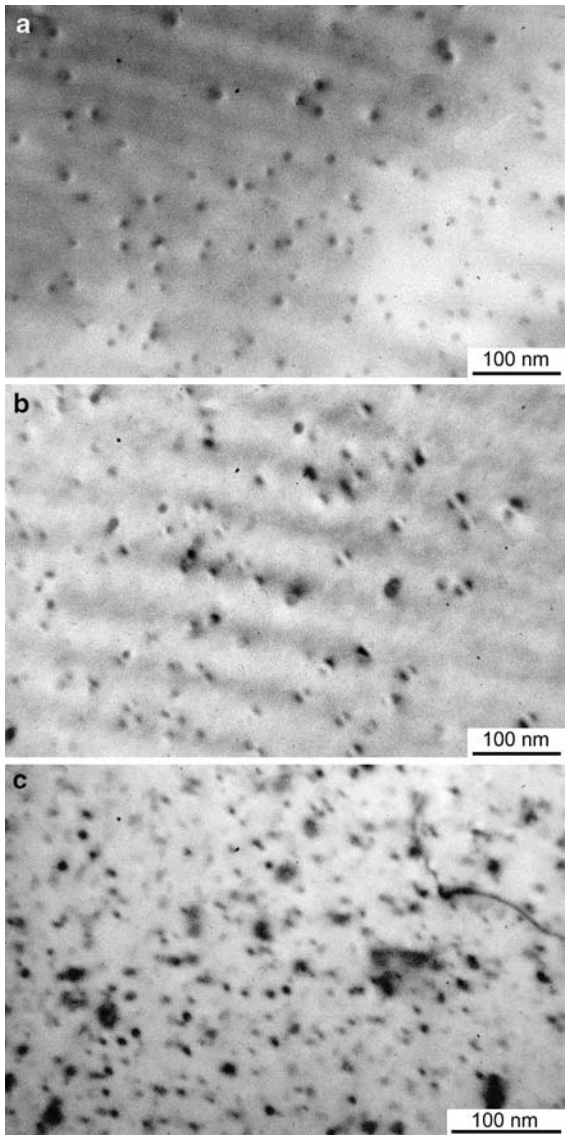

Fig. 5 Internal structure of Al–0.2% Zr (in this alloy there are fields completely free of precipitates that are not shown here) (**a**), Al–0.4% Zr (**b**), and Al–0.6% Zr (**c**) alloys cooled at V_{c2} (Table 1) annealed by regime S450 (Table 2)

the mean interparticle spacing or directly proportional to the volume fraction, if the distribution of precipitates is uniform and the size of particles remains unchanged [17]. The increase of hardening with increasing volume fraction of $Al_3(Sc, Zr)$ dispersoids, irrespective of the acting strengthening mechanism, has been previously demonstrated by Fuller et al. [4] and Kendig and Miracle [16]. The linear regression of the data reflecting the alloys with uniform dispersoids distribution gives the equation with regression coefficient $R = 0.997$:

$$\mathrm{HB} = 14.4 + 74.6Q_{\mathrm{v}}, \Delta\mathrm{HB} = 1.9,$$

where ΔHB is the statistical error.

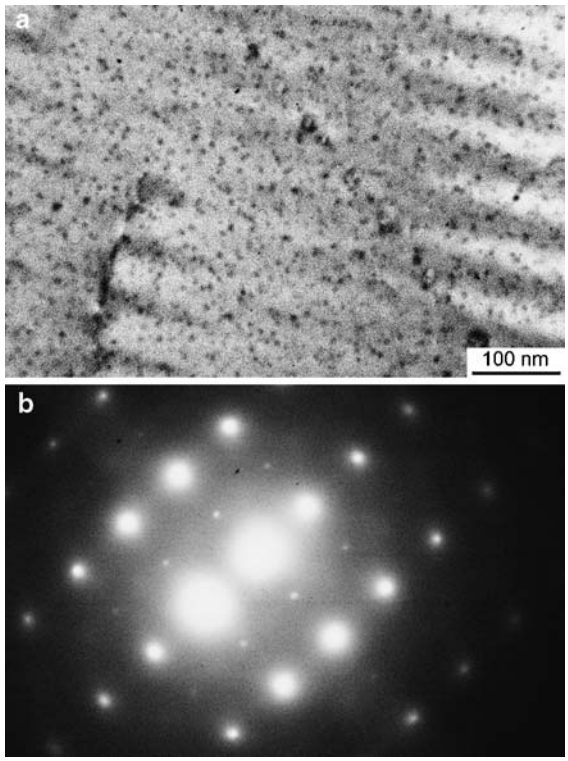

Fig. 6 Internal structure (**a**) and $(211)_{Al}$ selected-area electron diffraction pattern (**b**) of an Al–0.1% Sc–0.2% Zr alloys cooled at V_{c2} (Table 1) and annealed by regime S400 (Table 2)

The free member can be interpreted as the hardness of unalloyed aluminium, and the coefficient by Q_{v} as the hardness increment with 1 vol.% of precipitates added. This correlation is shown in Fig. 8 by a line. It is obvious that some experimental alloys fall out of this correlation. These are the alloys where precipitation occurs non-uniformly, i.e., Al–0.2% Zr (see Fig. 5a), Al–0.3% Sc–0.2% Zr (Fig. 7d), and Al–0.1% Sc–0.4% Zr, as well as the alloys where the precipitation density and size depend on the alloy composition as in Al–0.1% Sc and Al–0.5% Sc alloys [15]. This dependence also demonstrates that the full potential of precipitation hardening in the considered alloys can be achieved only by uniform distribution of precipitates. This uniform distribution is a function of composition, solidification conditions, and heat treating regime, and can be further assisted by partitioning of Sc and Zr during solidification [6].

One may conclude that only one alloy among the tested ternary alloys demonstrates uniform precipitation of dispersoids upon annealing to the maximum hardness, namely Al–0.1% Sc–0.2% Zr. A quantitative analysis of the internal structure shows that the precipitates in this alloy have an average diameter of 7 nm with a mean spacing of 50 nm at a volume fraction of 0.5 vol.%.

The hardening curves in Fig. 3 show that softening occurs on increasing the annealing temperature above

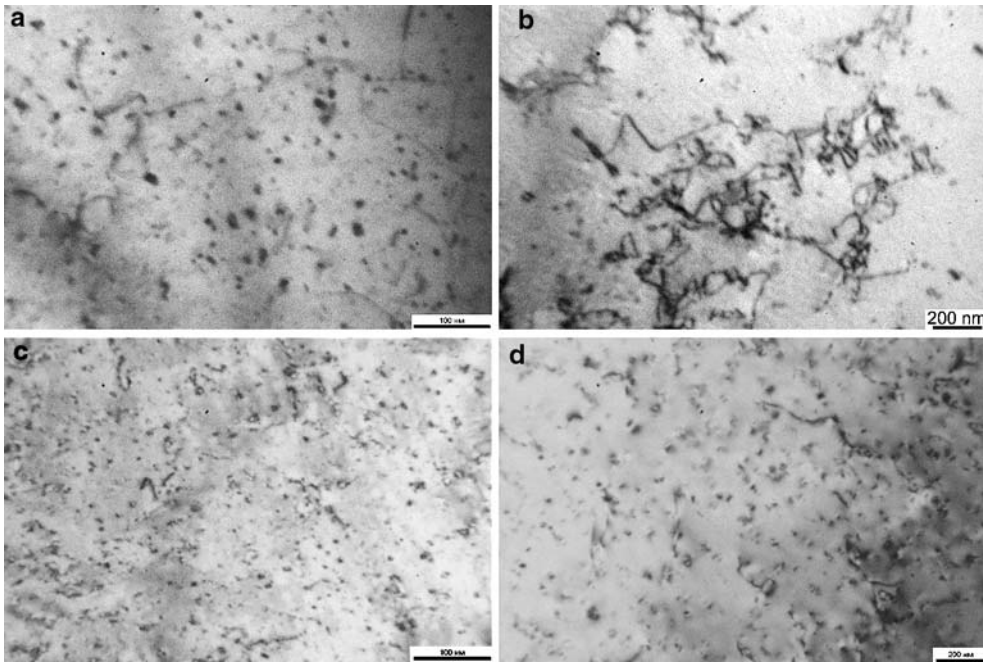

Fig. 7 Internal structure of an Al–0.3% Sc–0.2% Zr alloy in the as-cast state (**a**, **b**) and after annealing by regime S400 (Table 2) (**c**, **d**). Samples were cooled after the end of solidification at a rate of V_{c1} (**a**, **c**) and V_{c2} (**b**, **d**). See cooling schedule in Table 1

Table 3 Calculated volume fraction Q_v of dispersoids in experimental alloys

Zr, %	Sc, %	Phase	Q_v, vol.%
0.2	–	Al_3Zr	0.25
0.4	–	Al_3Zr	0.49
0.6	–	Al_3Zr	0.76
–	0.1	Al_3Sc	0.25
–	0.3	Al_3Sc	0.76
–	0.5	Al_3Sc	1.27
0.2	0.1	$Al_3(ScZr)$	0.5
0.4	0.1	$Al_3(ScZr)$	0.75
0.2	0.3	$Al_3(ScZr)$	1.01

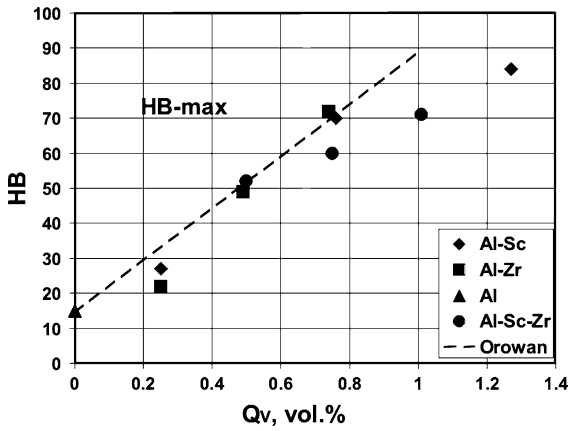

Fig. 8 Relationship between maximum hardness and volume fraction of precipitates in experimental alloys cooled at a cooling rate $\mathbf{V}_{c2}$. Line shows the best fit for the Orowan mechanism of hardening

400 °C. This softening is related to coarsening of precipitates. However, only precipitates with the cubic $L1_2$ structure are identified after annealing at up to 500 °C. At higher temperatures, severe coarsening is observed and the structure approaches the equilibrium. Low-alloyed materials, e.g., 0.1–0.3% Sc, 0.2% Zr, and 0.1% Sc + 0.2% Zr, appear to be single-phased solid solution after annealing by regime S640 (Table 2). This is in good agreement with the isothermal section in Fig. 1b. Binary Al–Zr alloys containing more than 0.4% Zr demonstrate faceted, rod-shaped crystals, apparently formed by the equilibrium tetragonal Al_3Zr phase, Fig. 9a. On the other hand, Fig. 9b shows that dispersoids in the binary Al–0.5% Sc alloy retain their spherical shape, as the precipitating phase does not change its structure. Two types of particles are observed in the ternary Al–0.3% Sc–0.2% Zr alloy, spherical and rod-like, Fig. 9c. This correlates well with the equilibrium phase composition of this alloy that requires the presence of two equilibrium phases Al_3Sc and Al_3Zr (see Fig. 1b).

The results presented in this work demonstrate that the maximum effect of hardening in aluminium alloys containing transition metals depends not only on the cooling rate during solidification, composition and annealing regime, but also on the casting temperature and the cooling rate after the end of solidification. The casting temperature should be chosen in such a way that the alloy is cast from above the liquidus of the highest-melting compound, Al_3Zr in Al–Sc–Zr alloys. The cooling rate after the end of solidification should be sufficient to prevent the precipitation of dispersoids during cooling. Figure 10 illustrates the effect of composition and cooling rate in the solid state on the possibility of decomposition during cooling. The time–temperature–transformation (TTT) curves of low-alloyed materials are on the right of the cooling curves, which

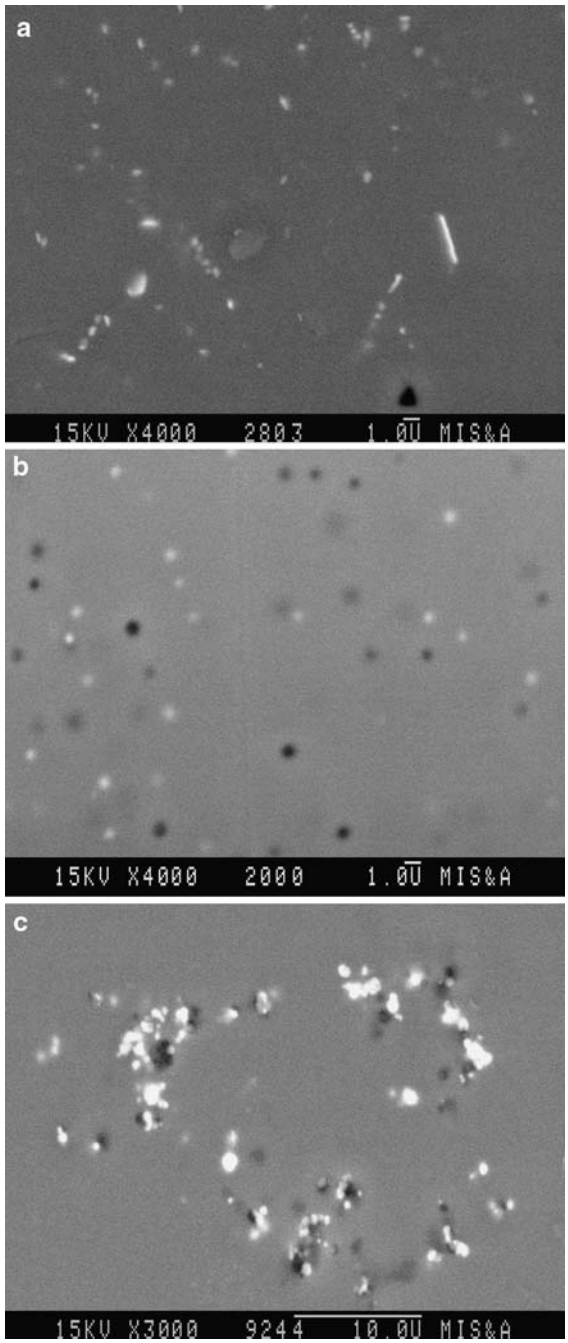

Fig. 9 Internal structure of alloys annealed by regime S640 (Table 1), SEM: (**a**) Al–0.4% Zr; (**b**) Al–0.5% Sc; and (**c**) Al–0.3% Sc–0.2% Zr

allows one to receive a single-phase supersaturated solid solution even at low cooling rates. Formation of the supersaturated solid solution in a more alloyed alloy, e.g., Al–0.6% Zr, requires a higher cooling rate. And high-alloyed materials, e.g. Al–0.3% Sc–0.2% Zr, are even more demanding for high cooling rates.

One can see that attempts to improve the hardening in Al–Sc–Zr alloys by simple boosting the alloying level are

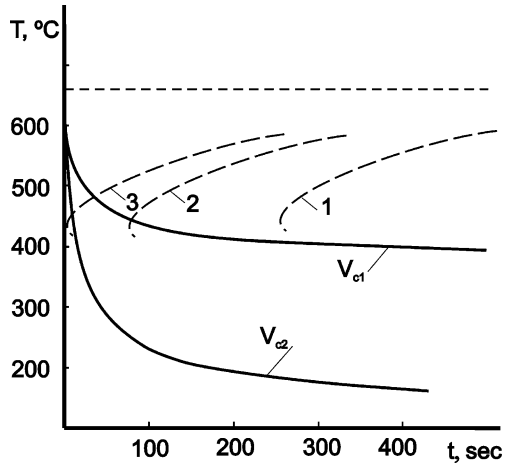

Fig. 10 Scheme of the ratio between cooling rates ($V_{c1} < V_{c2}$) and TTT-curves form low- (1), medium- (2) and high-alloyed (3) materials. Cooling curves are similar to those measured in experiments

not justified for the following reasons: (1) it becomes increasingly difficult to completely introduce alloying elements in the solid solution; (2) high concentrations of Sc and Zr mean high melting and cast temperatures, which in most cases makes such alloys unsuitable for commercial use; and (3) high-alloyed materials are prone to inhomogeneous distribution of precipitates, which decreases the efficiency of hardening.

The Al–0.1% Sc–0.2% Zr alloy shows adequate hardening level and temperature range (see Figs. 3 and 4), uniform precipitation (Figs. 6 and 8), and moderate sensitivity to the cooling rate in the solid state (Fig. 3c). The liquidus of this alloy is about 700 °C as shown in Fig. 1a that allows one to use normal casting technologies in producing this composition. The hardening of this alloy was tested on samples produced by casting from 750 and 700 °C. These samples were then annealed by regime 300 °C, 3 h + 400 °C, 3 h. In both cases, the hardness was

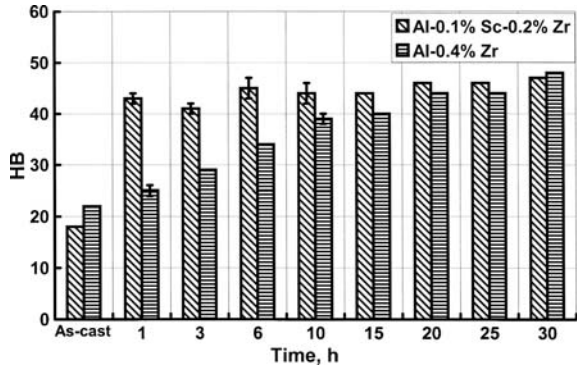

Fig. 11 Comparison of hardening at 300 °C in an Al–0.4% Zr alloy cast at 850 °C, V_{c2} and an Al–0.1% Sc–0.2% Zr alloy cast at 750 °C, V_{c2}.

similar to the maximum hardness shown by this alloy cast from 850 °C (see Fig. 3c). Figure 11 illustrates the hardening of this alloy at 300 °C as compared to the Al–0.4% Zr alloy. Note that the Al–Sc–Zr alloy was cast from the temperature 100 °C lower than the Al–Zr alloy. One can easily see that the Al–0.1% Sc–0.2% Zr alloy hardens faster and reaches the same maximum value as the Al–0.4% Zr alloys with the same volume fraction of precipitates (see Table 3).

Conclusions

The effects of composition, cooling rate in the solid state, and annealing temperature on hardening of binary and ternary alloys of the Al–Sc–Zr system are studied. It is shown that the hardening depends only on the volume fraction of precipitates in the case of their homogeneous distribution in the matrix. Non-uniform precipitation causes a decrease in hardening.

Medium- and high-alloyed materials are sensitive to the cooling rate after the end of solidification. It is found that such alloys can considerably harden as a result of decomposition of solid solution during cooling after the end of solidification. These alloys, however, demonstrate less hardening after subsequent annealing.

The liquidus of ternary Al–Sc–Zr alloys is experimentally assessed in this work and can be used in choosing correct melting and casting temperatures.

It can be recommended that the total concentration of Sc and Zr in commercial aluminium alloys, that are conventionally solution treated at 400–500 °C, does not exceed 0.3–0.4 wt% with the ratio Zr:Sc ≥ 2. This allows one to use normal casting temperatures, completely introduce Sc and Zr into solid solution during casting and subsequent cooling, fully use the hardening potential of the precipitates, and obtain considerable hardening during solution treatment.

Acknowledgement Authors would like to thank reviewers of this paper for their thorough reading and useful comments.

References

1. Toropova LS, Eskin DG, Kharakterova ML, Dobatkina TV (1998) Advanced aluminum alloys containing scandium: structure and properties. Gordon and Breach/OPA, Amsterdam
2. Forbord B, Lefebre W, Danoix F, Hallem H, Marthinsen K (2004) Scr Mater 51:333
3. Tolley A, Radmilovic V, Dahmen U (2005) Scr Mater 52:621
4. Fuller CB, Seidman DN, Dunand DC (2003) Acta Mater 51:4803
5. Forbord B, Hallem H, Marthinsen K (2004) In: Nie JF, Morton AJ, Muddle BC (eds) Proceedings of the 9th International Conference on Aluminium Alloys (ICAA'9), Brisbane, August 2004, p 1179
6. Robson JD (2004) Acta Mater 52:1409
7. Belov NA, Istomin-Kastrovskii VV, Naumova EA (1996) Izv Vyssh Uchebn Zaved Tsvetn Metall 4:45
8. Belov NA (1996) Mater Sci Forum 217–222:293
9. Belov NA, Zolotorevskii VS, Goto S, Alabin AN, Istomin-Kastrovskiy VV, Mishin VI (2004) In: Nie JF, Morton AJ, Muddle BC (eds) Proceedings of the 9th International Conference on Aluminium Alloys (ICAA'9), Brisbane, August 2004, p 533
10. Dobatkin VI (1970) In: Physical metallurgy of light alloys, Nauka, Moscow, p 100
11. Nes E, Billdal H (1977) Acta Metall 25:1031
12. Norman AF, Prangnell PB, McEwen RS (1998) Acta Mater 46:5715
13. Novotny GM, Ardell AJ (2001) Mater Sci Eng A A318:144
14. Nakayama M, Furuta A, Miura Y (1997) Mater Trans JIM 38:852
15. Marquis EA, Seidman DN (2001) Acta Mater 49:1909
16. Kendig KL, Miracle DB (2002) Acta Mater 50:4165
17. Martin JW (1980) Micromechanisms in particle-hardened alloys. Cambridge University Press, Cambridge